Minimal climate impacts from short-lived climate forcers following emission reductions related to the COVID-19 pandemic.

James Weber[1], Youngsub Matthew Shin[2], John Staunton Sykes[2], Scott Archer-Nicholls[3], Nathan Luke Abraham[4], and Alexander Thomas Archibald[3]

[1]Centre for Atmospheric, Department of Chemistry, University of Cambridge
[2]Centre for Atmospheric Science, Department of Chemistry, University of Cambridge
[3]University of Cambridge
[4]NCAS, University of Cambridge

November 24, 2022

Abstract

We present an assessment of the impacts on atmospheric composition and radiative forcing of short-lived pollutants following worldwide decrease in anthropogenic activity and emissions comparable to what has occurred in response to the COVID-19 pandemic, using the global composition-climate model UKCA. Changes in emissions reduce tropospheric hydroxyl radical and ozone burdens, increasing methane lifetime. Reduced SO emissions and oxidising capacity lead to a decrease in the sulphate aerosol burden and increase in aerosol particle size, with accompanying reductions to cloud droplet number concentration. However, large reductions in black carbon emissions increase the albedo of aerosols. Overall, the changes in ozone and aerosol direct effects (neglecting aerosol-cloud interactions) result in an instantaneous radiative forcing of -31 to -74 mWm. Upon cessation of emission reductions the short-lived climate forcers rapidly return to pre-COVID levels, meaning these changes are unlikely to have lasting impacts on climate assuming emissions return to pre-intervention levels.

Minimal climate impacts from short-lived climate forcers following emission reductions related to the COVID-19 pandemic

James Weber[1], Youngsub M. Shin[1], John Staunton Sykes[1], Scott Archer-Nicholls[1], Nathan Luke Abraham[1,2] and Alex T. Archibald[1,2]

[1]Centre for Atmospheric Science, Department of Chemistry, University of Cambridge, Cambridge, CB2 1EW, UK
[2]National Centre for Atmospheric Science, Department of Chemistry, University of Cambridge, Cambridge, CB2 1EW, UK

Corresponding authors:
James Weber (jmw240@cam.ac.uk)
Youngsub M. Shin, (yms23@cam.ac.uk)
John Staunton Sykes (jjas3@cam.ac.uk)

Key Points:

- Emission reductions are likely to have led to a global reduction in short-lived climate forcers and tropospheric oxidising capacity.
- Reductions in O_3 and aerosol from both lower emissions and decreased sulphate oxidation resulted in a net negative radiative forcing.
- The radiative impacts are small and short-lived. Longer term climate impacts must come through future sustained emission reductions.

Abstract

We present an assessment of the impacts on atmospheric composition and radiative forcing of short-lived pollutants following worldwide decrease in anthropogenic activity and emissions comparable to what has occurred in response to the COVID-19 pandemic, using the global composition-climate model UKCA. Changes in emissions reduce tropospheric hydroxyl radical and ozone burdens, increasing methane lifetime. Reduced SO_2 emissions and oxidising capacity lead to a decrease in the sulphate aerosol burden and increase in aerosol particle size, with accompanying reductions to cloud droplet number concentration. However, large reductions in black carbon emissions increase the albedo of aerosols. Overall, the changes in ozone and aerosol direct effects (neglecting aerosol-cloud interactions) result in an instantaneous radiative forcing of -31 to -74 mWm^{-2}. Upon cessation of emission reductions, the short-lived climate forcers rapidly return to pre-COVID levels, meaning these changes are unlikely to have lasting impacts on climate assuming emissions return to pre-intervention levels.

Plain Language Summary

As a result of the global COVID-19 pandemic, unprecedented lockdown measures have been imposed worldwide to reduce the spread of the disease, causing huge reductions in economic activity and corresponding reductions in transport, industrial and aviation emissions. As well as lowering emissions of long lived greenhouse gases, such as carbon dioxide, this has resulted in a dramatic reduction in the emissions of components which affect climate in the short term. In this study we have used state-of-the-art computer simulations to quantify how changes in these components are likely to impact the chemical make-up of the atmosphere and the likely short-term impacts on climate. Despite large decreases in nitrogen dioxide and atmospheric particles, we find these changes result in a very small impact on the energy balance of the atmosphere but one that would act to cool the planet, without considering the knock-on impacts on clouds. However, these effects are all likely to be short-lived if emissions return to pre-lockdown levels.

1 Introduction

The outbreak of the COVID-19 coronavirus disease in China in December 2019 and its global spread in early 2020 has led to the most deadly and disruptive pandemic in recent memory. As of 8 June, there have been 6.8 million confirmed cases and 395,000 deaths globally (WHO). In response, governments around the world have implemented varying lockdown measures. The resulting decreases in transport and economic activity have led to the unprecedented reduction of anthropogenic emissions of carbon dioxide (CO_2) (Le Quéré, 2020) and short-lived climate forcers (SLCF) (Zhang et al., 2020). The SLCFs include sulphur dioxide (SO_2), nitrogen oxides (NO and NO_2, which together form NO_x), carbon monoxide (CO), and organic carbon and black carbon (OC and BC respectively). Such species perturb the oxidant balance of the atmosphere (O'Connor et al., 2020), the ozone budget (Young et al., 2018) and aerosol burden (Karset et al., 2018), and thus the radiative balance of the atmosphere and climate (Myhre et al., 2013). This paper aims to assess how the perturbations to atmospheric composition arising from changes to emissions of SLCFs due the COVID-19 pandemic affect parameters important for climate.

There remains uncertainty in the temporal, spatial, and composition changes to emissions arising from the restrictions imposed. Le Quéré et al (2020) calculated reductions in daily CO_2 emissions of between 11 and 25% by April 2020 relative to April 2019. Despite this uncertainty there exists common themes to emissions changes on which this study focuses.

2 Methods

2.1 Model description

Five experiments were performed using the United Kingdom Chemistry and Aerosols Model (UKCA) run at a horizontal resolution of 1.25°×1.9° with 85 vertical levels up to 85 km (Walters et al., 2019) with the fully interactive stratospheric and tropospheric chemistry (Archibald et al., 2020), and GLOMAP-mode aerosol scheme which simulates sulphate, sea-salt, black carbon, organic matter, and dust but not currently nitrate aerosol (Mulcahy et al., 2020). Emissions were from the CMIP6 CEDS inventories (Hosely et al. 2018). Emissions of methane (CH_4) and carbon dioxide (CO_2) were not simulated, rather a prescribed value is applied for CO_2 and a lower

boundary condition (fixed surface concentration) used for methane. The simulations were run using nudging (Telford et al., 2008) to atmospheric reanalyses from ECMWF (Dee et al., 2011) to constrain the simulations to consistent meteorology enabling a small ensemble of three different years: 2012, 2013, and 2014. The years chosen were the most recent CMIP6 emissions available at the time, and were averaged to filter out the influence of interannual meteorological variation. Nudging prevented temperatures and horizontal winds from responding to the forcings produced by the emissions changes, thus preventing changes in aerosols from affecting clouds and the subsequent impacts on the radiation budget (Zhang et al., 2014).

2.2 Scenario descriptions

Five scenarios were considered, each with different perturbations to emissions (Table 1). Emitted species are specified in Table S1. The perturbation scenarios A1-A4 were developed by reducing global anthropogenic emissions in the aviation, surface transport, and industrial sectors by a set factor. In all perturbation scenarios, emissions were held at the control run values until mid-February before declining linearly until mid-March to their minimum value. They remained at their minimum value until mid-May before increasing linearly to the control levels by mid-June (Fig. S1). We made the approximation of all countries in the world making parallel emission reductions. As these scenarios were developed early in the COVID-19 pandemic when information on the impact of the lockdown on all sectors was unknown, we drew on available information from a number of sources to compile emission reduction scenarios that span likely representative changes in emissions. See Text S1 for further details.

Table 1 - Scenarios and emission changes

Scenario	**Transport**	**Aircraft**	**Industry**	**% Global change in surface emissions during "lockdown period" (March-May)**			
				NO	SO_2	BC	OC
Control	No reduction	No reduction	No reduction	No reduction	No reduction	No reduction	No reduction
A1	-50%	-50%	-25%	-15.8	-8.84	-11.88	-3.66
A2	-50%	-25%	-25%	-15.8	-8.84	-11.88	-3.66
A3	-75%	-50%	-25%	-22.2	-9.48	-16.48	-4.52
A4	-50%	-50%	No reduction	-12.8	-1.27	-9.19	-1.73

The scenarios were designed to allow a comparison between the effects of decreasing different sectors on emissions. By comparing A1 with A3 and A4, we saw that global NO_x emissions were

approximately twice as sensitive to surface transport emissions than industrial emissions, while the majority of SO_2 emission decreases were due to industrial emissions. Comparing the primary aerosol emissions, BC was more sensitive to the surface transport sector, whilst OC was more sensitive to industry. While reducing aviation emissions resulted in a negligible decrease in the total mass of emissions, these emissions were injected directly into the free troposphere which is more sensitive to NOx emissions (Stevenson et al., 2004). These reductions are in line with those in the recently published study by Le Quéré et al (2020) which estimates decreases in aviation of 50-90%, in surface transport of 40-75% and various industrial emissions such as Chinese coal (40%) and US steel (35%).

3 Results

In all cases we combined the results from the simulations with different years of meteorology to generate an ensemble mean, and compared the results of the different scenarios (A1-A4) to the control case. In all the scenarios the effects of emissions changes were short lived and atmospheric composition returned to control levels within a couple months of the emissions reductions ceasing. In the following analyses we focus on the lockdown period (mid-March to mid-May), where emissions are prescribed to be at their lowest, and quantify changes in composition and average instantaneous radiative forcing (IRF) from O_3 and aerosol direct effects.

3.1 Evaluation of NO_2 Column

Observations of tropospheric NO_2 columns have exhibited significant reductions globally (Bauwens et al., 2020, Zhang et al., 2020) with decreases in excess of 20% over many major cities. Figures 1 and S2 show NO_2 column changes from observation (Bauwens et al., 2020) and model scenarios.

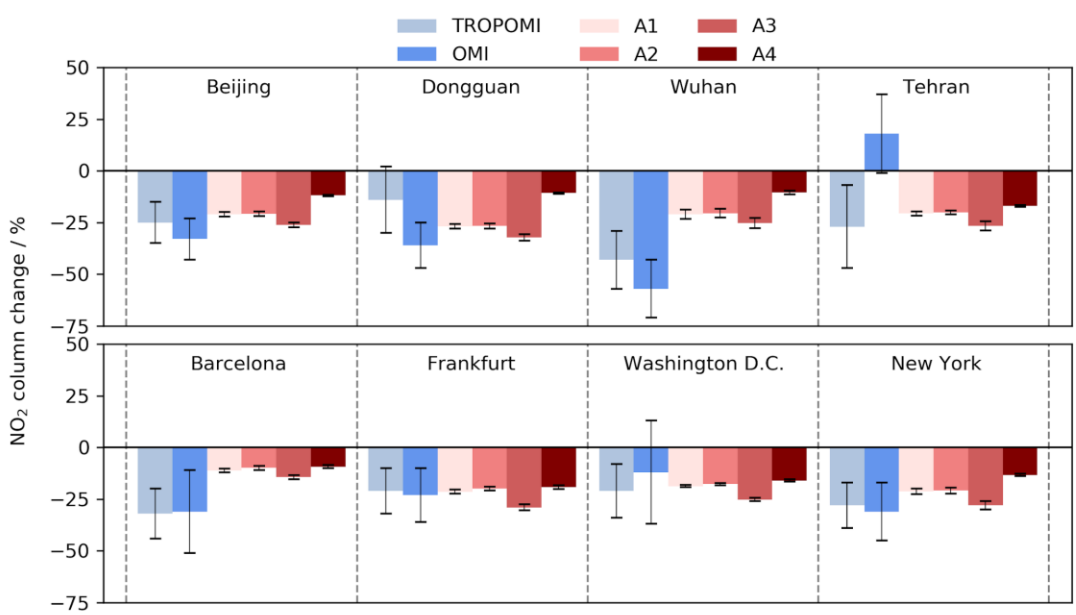

Figure 1. Observed and modelled tropospheric NO_2 column changes. Observations are from TROPOMI and OMI relative to 2019, see Bauwens et al. (2020) for more details. Model results are from the 4 scenarios relative to the control averaged over the period of lowest emissions (mid-March to mid-May).

Figure 1 highlights that our model simulations are in good agreement with observed NO_2 column decreases by Bauwens et al. (2020), with the A1 scenario being within error in most cases. This increases confidence in the representativeness of our emissions scenarios for the COVID-19 changes. However, we note that the model simulations generally underestimate the magnitude of NO_2 column changes, suggesting our emission perturbations may be at the lower end of what happened during the pandemic. Shi and Brasseur (2020) showed through surface observation analyses across China that the COVID-19 lockdowns resulted in significant decreases in NO_2, but increases in ozone (O_3). These local increases in surface O_3 in polluted regions are also captured in our simulations, although with a smaller magnitude (Fig. 2), and are driven by the non-linear NO_x-VOC chemistry that produces O_3 in the troposphere (Monks et al., 2016). However, all scenarios exhibited a general decrease in global tropospheric O_3, attributed to the reduction in NO_x emissions.

3.2 Reduction in Oxidant Burden

Globally averaged, the changes to emissions from transport, industry and aviation led to decreases in the tropospheric O_3 burden of 2.0-3.2 % (Fig. 2, S3), which recovered quickly once emissions increased. The OH concentration was also simulated to have decreased (Fig. 2). The reduction in tropospheric O_3 was most pronounced in A3 where localised decreases exceeded 7%, illustrating the large impact of reducing surface transport emissions. The Northern Hemisphere midlatitudes, the location of the largest absolute change in emissions, saw the greatest reductions. Spatial heterogeneity in OH and O_3 depletion between scenarios revealed the importance of emissions from surface transport and aviation (Fig. S4). The additional decreases in low altitude O_3 and OH in Scenario A3 relative to A1 were attributed to the greater reduction in surface transport emissions in A3, while smaller decreases in mid altitude O_3 and OH in A2 were due to the smaller reduction in aviation emissions. The similarity in O_3 and OH between scenarios A1 and A4 signified the tropospheric oxidant budget is relatively insensitive to industrial emissions.

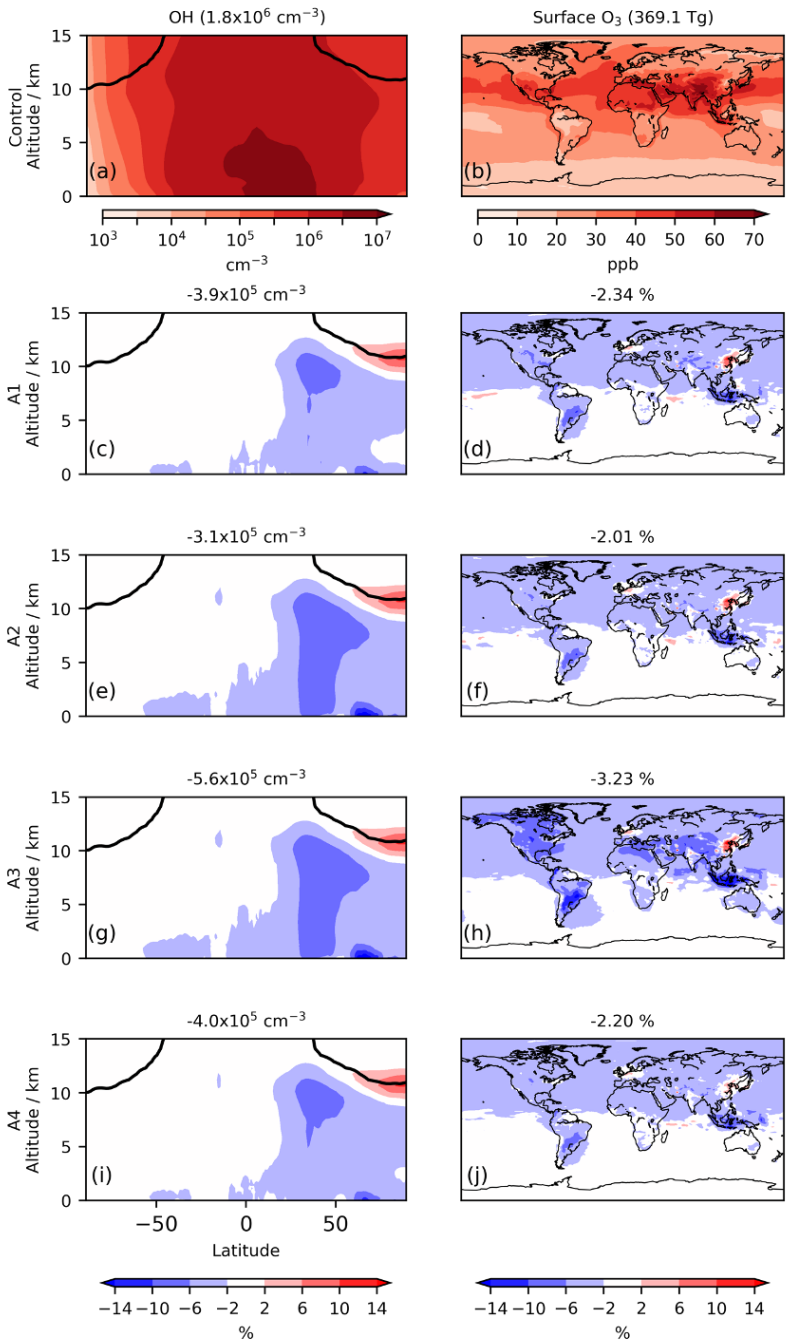

Figure 2. Zonal mean OH and surface O_3 mixing ratios in control runs and respective changes (mid-March to mid-May). Model results are the ensemble mean for each scenario. Black lines in the OH plots show the tropopause. Titles in the left column show mean tropospheric air-mass-weighted [OH] in control (top) and change (lower panels). Titles in the right column show mean tropospheric O_3 burden in control (top) and change (lower panels).

The decrease in tropospheric OH did not affect model methane concentration due to the fixed methane surface boundary condition. However, the change in methane concentration, c, which

would have occured can be calculated from the methane lifetime (Eq.1) (Thornhill et al., 2020), where f=1.33 is methane's feedback on its own lifetime (Fiore et al., 2009).

$$\frac{\Delta c}{c} = (\frac{\Delta\tau}{\tau} + 1)^f - 1 \approx f\frac{\Delta\tau}{\tau}$$

Equation 1

Methane lifetime increased by 2-2.5% (A1-2, A4) and 4% (A3) over the period of emissions reduction (Fig. S5). This would correspond to increases in methane concentration of ~20-40 ppb if steady state were reached. However, given the perturbations' brevity, much smaller increases of 1-2 ppb were calculated as an upper bound (Text S2). We therefore conclude the effect on methane concentration and the associated forcing are negligible.

3.3 Reduction in Sulphate Aerosol Burden

The perturbation to oxidants reduced the oxidation flux of SO_2 beyond the change due to the reduction in SO_2 emissions alone, illustrating the coupling between emissions, oxidants and sulphate aerosol, an important climatic forcer. SO_2 production fluxes (emissions plus chemical production) decreased by around 8% (A1-A3) and 1.3% (A4), highlighting the sensitivity of SO_2 to industrial emission reductions. However, the corresponding drop in SO_2 burden (5.4% (A1-A3) and 0.1% (A4)) (Fig. 3(a)) was smaller than the production flux decrease due to a reduction in chemical loss driven by oxidant decreases. This effect was most pronounced with the tropospheric gas phase OH + SO_2 flux which decreased by 8-9.5% (A1-A3) and 2.6% (A4) (Fig. 3(b)) and showed significant spatial similarity to [OH] change and exceeded the changes in SO_2 alone (Fig. S5).

The other SO_2 oxidation pathway, aqueous oxidation by H_2O_2 and O_3, decreased by only 4% (A1-A3), meaning relatively more SO_2 was oxidised via aqueous phase chemistry. This is important because in UKCA, the H_2SO_4 produced via OH + SO_2 oxidation can nucleate new particles and thus affects aerosol number and size distribution. However, the aqueous phase pathway only adds mass to existing particles. The different reductions in gaseous and aqueous flux causes an additional perturbation to the aerosol size distribution resulting in fewer, larger aerosols (Fig. 3 (c, e)).

We calculated a reduction in sulphate aerosol burden (with rapid post-lockdown recovery) with non-uniform reduction across the aerosol modes and largest changes in the mid latitude Northern Hemisphere (Figs. S6,7). The largest decrease in mass occurred in the accumulation mode (Fig. 3(c)) and the largest decrease in number in the nucleation mode (Fig. 3(d)). This perturbation to the size distribution produced an increase in the mean aerosol effective radius (r_{eff}) of 1-4% (Fig. 3(e)) and is attributed in part to the greater relative reduction of gas phase oxidation of SO_2 (and thus new particle nucleation) than aqueous phase oxidation: a further illustration of coupling between composition and climatically-relevant agents.

The perturbation to the aerosol size and number distribution resulted in cloud droplet number concentration (CDNC) decreases of up to 4% globally (Fig. 3(f)), with localised decreases exceeding 10% (Fig. S8) and commensurate increase in effective cloud droplet radius of 0.25-0.4% (Figs. S9, S10). The drop in CDNC is likely to reduce cloud albedo (Twomey, 1977) and thus contribute a positive forcing but this has not been calculated here.

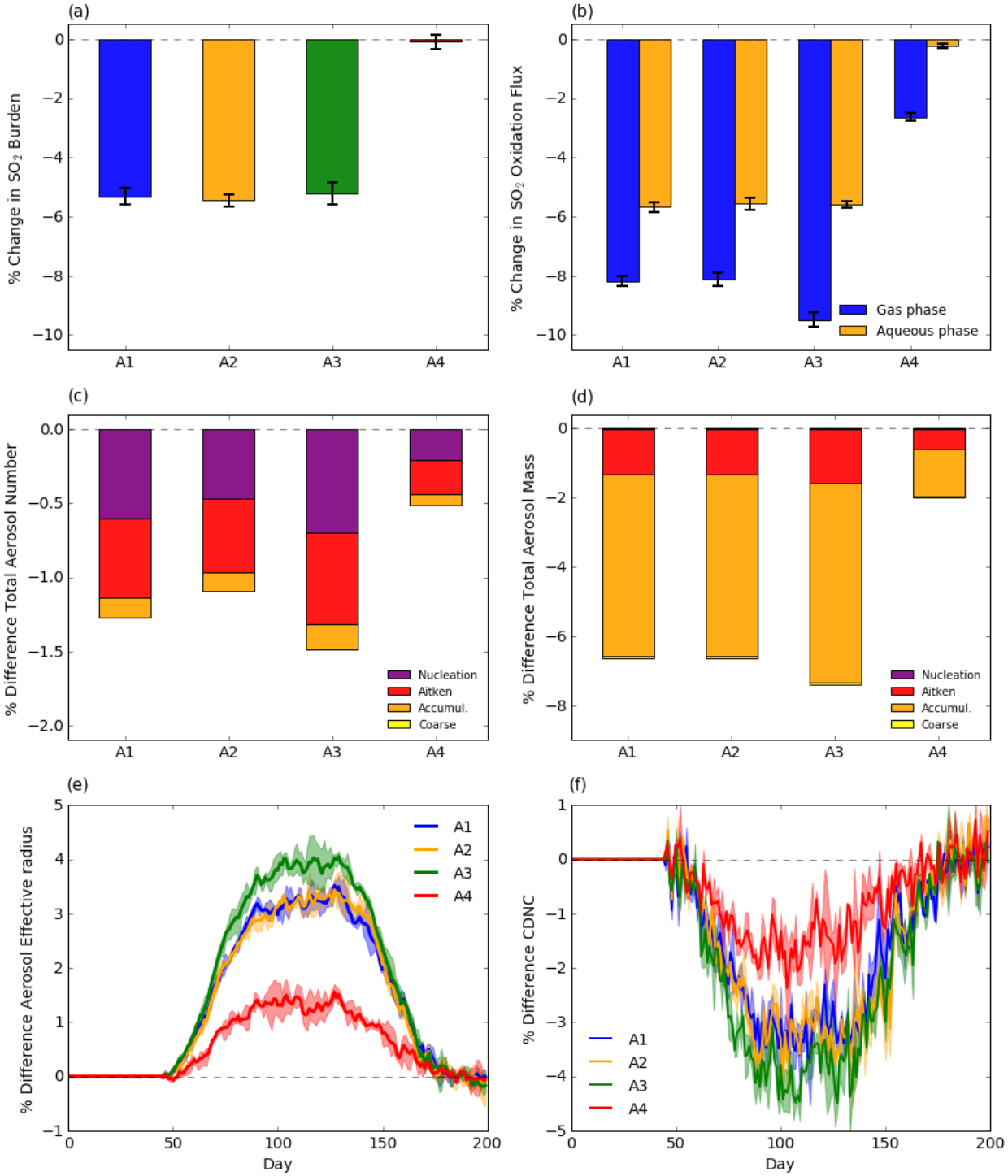

Figure 3 - Mean change in (a) SO_2 burden, (b) SO_2 oxidation flux, (c) sulphate aerosol number, and (d) mass burden split by aerosol size (March to May). Mean change in (e) r_{eff} and (f) CDNC (error bars and shading show ensemble range).

3.4 Aerosol Optical Depth

The decrease in simulated sulphate aerosol burden and emissions of primary aerosol (BC, OC) results in decreases in aerosol optical depth (AOD) at 550 nm across most terrestrial regions in scenarios A1-A3 (Fig. S11) with rapid increase upon emission increase. Eastern China exhibits the largest absolute decreases (Fig. S12) while A4 showed much smaller decreases, highlighting the major contribution of industrial SO_2 emissions to AOD. Observed AOD changes between 2017-2019 and 2020 from VIIRS (Sayer et al., 2018) were analysed (Fig. S13) but showed little significant sign due to considerable noise.

4. Radiative Effects

The impact of ozone reduction (Fig. S14) was estimated using the conversion factor of 0.042 Wm^{-2} DU^{-1} (Stevenson et al., 2013). The IRF resulting from aerosol direct radiative effects, IRF_{DRE}, was calculated by comparing the total outgoing flux, F, and outgoing clean air flux, F_{clean}, between the perturbed and control runs (Eq. 2) following Ghan (2013).

$$IRF_{DRE} = \Delta(F - F_{clean})$$

Equation 2

The IRF_{DRE} was calculated to be significantly smaller than the O_3 forcings in A1 and A2 but comparable in A3 and A4. Despite the warming effect expected from the reduction in sulphate aerosol, the global aerosol IRF was simulated to be negative in all scenarios (Table 2).

Table 2 - IRF relative to control runs averaged over period of lowest emissions (mid March - mid May).
Values in parentheses show the ensemble range.

Instantaneous Radiative Forcing / mWm^{-2}	**A1**	**A2**	**A3**	**A4**
Ozone	-34 (-37 to -31)	-29 (-32 to -27)	-47 (-50 to -43)	-32 (-35 to -30)
Aerosol Direct Effect IRF	-4 (-9 to +3)	-2 (-8 to +6)	-27 (-34 to -18)	-44 (-47 to -40)
Ozone and Aerosol IRF	-38	-31	-74	-66

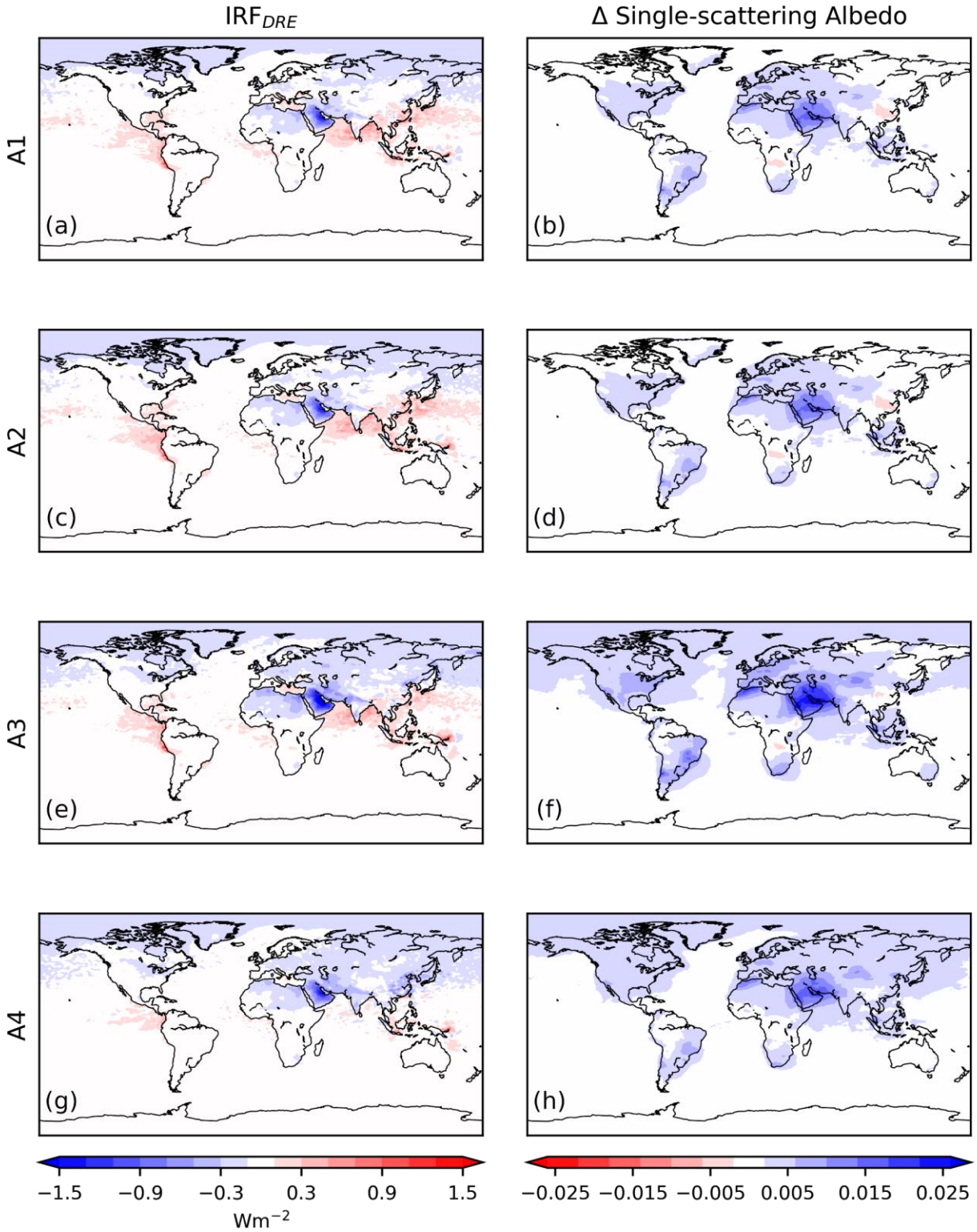

Figure 4. IRF from aerosol direct effects (IRF_{DRE}) and change in single-scattering albedo (March to May) averaged over the 3 years investigated.

Spatial analysis of the IRF_{DRE} (Fig. 4) revealed a negative forcing over large Northern Hemisphere continental regions except Eastern China, the location of the greatest reduction in SO_2 emissions, which exhibited a warming in A1-A3. This warming was attributed to SO_2 emission reductions associated with industry as it was not simulated in A4.

The negative forcing was especially strong over the Arabian peninsula. This was attributed to the fact that the reduction in aerosol exposed solar radiation to a surface with a higher albedo than the original aerosol population, resulting in a greater fraction of insolation being reflected (Haywood and Shine., 1995). This effect was compounded on the Arabian peninsula by the large decreases in black carbon emissions from both surface transport and industry sectors (Fig. S16), a strongly absorbing aerosol component with low single-scattering albedo (Bond et al., 2013). Accordingly, the increase in single-scattering albedo (Fig. 4) is most pronounced over the Arabian peninsula and correlates well with the negative IRF_{DRE}. In addition, the reduction in SO_2 emissions (Fig. S14) was much more modest in this region and therefore the associated warming effects were smaller. Globally these competing aerosol forcing effects almost completely offset in A1 and A2 while the greater reductions in black carbon from surface transport resulted in net cooling in A3. The even larger cooling in A4 was attributed to the combination of BC emissions reduction from transport with the much smaller reduction in SO_2 emissions without industry mitigation, resulting in higher aerosol SSA and a negative forcing.

5. Conclusion

In this study we investigated the impacts on atmospheric composition and radiative forcing from changes in anthropogenic road transport, aviation, and industrial emissions comparable to those resulting from the response to the COVID-19 pandemic. Our model results have shown these emission reductions led to significant changes in atmospheric composition, driven by the changes in the oxidising capacity of the troposphere and oxidant-aerosol-precursor interactions. Decreases in NO_x emissions reduced tropospheric O_3 and as a result the oxidising capacity, with concomitant increases in methane lifetime although a negligible increase in methane forcing. SO_2 emission reductions and the reduction in tropospheric oxidising capacity led to decreases in sulphate burden. The reduction in sulphate aerosol number is predominantly manifest in the nucleation mode; attributed in part to the greater relative reduction in gas phase SO_2 oxidation compared to aqueous phase oxidation and supported by increases in aerosol effective radius and decreases in CDNC. This highlights the influence of oxidant changes on the aerosol size distribution (as well as aerosol burden), an important climatic parameter.

Despite reduction in the sulphate aerosol burden, decreases in BC emissions resulted in a negative forcing from the aerosol direct effect which, when combined with the negative forcing from tropospheric O_3 reduction, led to a small negative forcing of 31-74 mWm^{-2}. This change is short-lived and comparable to a *temporary* decrease of 3-6 ppm of CO_2. Due to model setup limitations these estimates do not include impacts from aerosol-cloud interactions. However we can speculate from the reductions in aerosol number and CDNC that cloud effects would have a

positive forcing, reducing the overall magnitude of the forcing we calculated and potentially changing its sign.

Our results suggest that temporary changes to SLCF emissions due to the COVID-19 emergency measures are not going to have a significant impact on near-term climate change, implying that changes in CO_2 emissions during the lockdown period and following recovery will be more important in determining the lasting impact of the pandemic on climate. Elucidating the full effective radiative forcing, including aerosol-cloud interactions, and the climate response due to emission changes warrants further investigation using longer free-running simulations.

Acknowledgements: JW would like to thank the Cambridge Commonwealth, European & International Trust for funding through a Vice Chancellor's Award; YMS and JSS would like to thank NERC through the University of Cambridge ESS-DTP for funding. We would like to thank NERC, through NCAS, and the Met Office for the support of the JWCRP UKCA project. SA and ATA would like to thank NERC PROMOTE (NE/P016383/1). NLA and ATA are supported by NERC and NCAS through the ACSIS project. This work used Monsoon2, a collaborative High Performance Computing facility funded by the Met Office and the Natural Environment Research Council. This work used JASMIN, the UK collaborative data analysis facility. We would also like to thank Dr Dan Grosvenor and Dr Paul Griffiths for their advice.

Competing Interests: All authors declare that they have no competing interests.

Author contributions: JW, YMS and JSS led the experimental design and analysis in the study. All co-authors contributed to writing and reviewing the manuscript.

Data availability: All necessary data is in the process of being deposited on the CEDA archive https://arrivals.ceda.ac.uk/uploader/browse/Covid-19_emiss_reduc_study/

References

Archibald, A. T., O'Connor, F. M., Abraham, N. L., Archer-Nicholls, S., Chipperfield, M. P., Dalvi, M., Folberth, G. A., Dennison, F., Dhomse, S. S., Griffiths, P. T., Hardacre, C., Hewitt, A. J., Hill, R. S., Johnson, C. E., Keeble, J., Köhler, M. O., Morgenstern, O., Mulcahy, J. P., Ordóñez, C., Pope, R. J., Rumbold, S. T., Russo, M. R., Savage, N. H., Sellar, A., Stringer, M., Turnock, S. T., Wild, O., and Zeng, G.: (2020) Description and evaluation of the UKCA stratosphere–troposphere chemistry scheme (StratTrop vn 1.0) implemented in UKESM1, Geosci. Model Dev., 13, 1223–1266, https://doi.org/10.5194/gmd-13-1223-2020.

Bauwens, M., Compernolle, S., Stavrakou, T., Müller, J.F., van Gent, J., Eskes, H., Levelt, P.F., van der A, R., Veefkind, J.P., Vlietinck, J. and Yu, H. (2020). Impact of coronavirus outbreak on NO2 pollution assessed using TROPOMI and OMI observations. *Geophysical Research Letters*, https://doi.org/10.1029/2020GL087978

Dee, D.P., Uppala, S.M., Simmons, A.J., Berrisford, P., Poli, P., Kobayashi, S., Andrae, U., Balmaseda, M.A., Balsamo, G., Bauer, P., Bechtold, P., Beljaars, A.C.M., van de Berg, L., Bidlot, J., Bormann, N., Delsol, C., Dragani, R., Fuentes, M., Geer, A.J., Haimberger, L., Healy, S.B., Hersbach, H., Hólm, E.V., Isaksen, L., Kållberg, P., Köhler, M., Matricardi, M., McNally, A.P., Monge-Sanz, B.M., Morcrette, J.-J., Park, B.-K., Peubey, C., de Rosnay, P., Tavolato, C., Thépaut, J.-N. & Vitart, F. (2011). The ERA-Interim reanalysis: configuration and performance of the data assimilation system. *Q.J.R. Meteorol. Soc.* https://doi:10.1002/qj.828

Bond, T.C., Doherty, S.J., Fahey, D.W., Forster, P.M., Berntsen, T., DeAngelo, B.J., Flanner, M.G., Ghan, S., Kärcher, B., Koch, D. and Kinne, S. (2013). Bounding the role of black carbon in the climate system: A scientific assessment. *Journal of Geophysical Research: Atmospheres*. https://doi.org/10.1002/jgrd.50171.

European Environment Agency. (2020). Air pollution goes down as Europe takes hard measures to combat coronavirus, viewed 5th April 2020, https://www.eea.europa.eu/highlights/air-pollution-goes-down-as.

Fiore, A. M., Dentener, F. J., Wild, O., Cuvelier, C., Schultz, M. G., Hess, P., Textor, C., Schulz, M., Doherty, R. M., Horowitz, L. W., MacKenzie, I. A., Sanderson, M. G., Shindell, D. T., Stevenson, D. S., Szopa, S., Van Dingenen, R., Zeng, G., Atherton, C., Bergmann, D., Bey, I., Carmichael, G., Collins, W. J., Duncan, B. N., Faluvegi, G., Folberth, G., Gauss, M., Gong, S., Hauglustaine, D., Holloway, T., Isaksen, I. S. A., Jacob, D. J., Jonson, J. E., Kaminski, J. W., Keating, T. J., Lupu, A., Manner, E., Montanaro, V., Park, R. J., Pitari, G., Pringle, K. J., Pyle, J. A., Schroeder, S., Vivanco, M. G., Wind, P., Wojcik, G., Wu, S. & Zuber, A. (2009) Multimodel estimates of intercontinental source-receptor relationships for ozone pollution. *J. Geophys. Res. Atmos.* https://doi:10.1029/2008JD010816.

Flight Radar (2020) Charting the decline in air traffic caused by COVID-19, viewed 1 June 2020, https://www.flightradar24.com/blog/charting-the-decline-in-air-traffic-caused-by-covid-19/.

Haywood, J.M. and Shine, K.P. (1995). The effect of anthropogenic sulfate and soot aerosol on the clear sky planetary radiation budget. *Geophysical Research Letters*. https://doi.org/10.1029/95GL00075

Hoesly, R.M., Smith, S.J., Feng, L., Klimont, Z., Janssens-Maenhout, G., Pitkanen, T., Seibert, J.J., Vu, L., Andres, R.J., Bolt, R.M. and Bond, T.C. (2018). Historical (1750–2014) anthropogenic emissions of reactive gases and aerosols from the Community Emissions Data System (CEDS). *Geoscientific Model Development (Online)*, https://10.5194/gmd-11-369-2018

Karset, I.H.H., Berntsen, T.K., Storelvmo, T., Alterskjær, K., Grini, A., Oliviè, D.J.L., Kirkevåg, A., Seland, Ø., Iversen, T. and Schulz, M. (2018). Strong impacts on aerosol indirect effects from historical oxidant changes. *Atmospheric Chemistry and Physics*, https://doi.org/10.5194/acp-18-7669-2018

Kommenda, N. (2020), How is the coronavirus affecting global air traffic?, viewed 1 June 2020, https://www.theguardian.com/world/ng-interactive/2020/apr/03/how-is-the-coronavirus-affecting-global-air-traffic

Le Quéré, C., Jackson, R.B., Jones, M.W., Smith, A.J., Abernethy, S., Andrew, R.M., De-Gol, A.J., Willis, D.R., Shan, Y., Canadell, J.G. and Friedlingstein, P. (2020). Temporary reduction in daily global CO 2 emissions during the COVID-19 forced confinement. *Nature Climate Change*, https://doi.org/10.1038/s41558-020-0797-x

Mallet, V (2020), EU carbon emissions tumble during lockdown, viewed 10th April 2020. https://www.ft.com/content/4c59fd16-6020-4798-b8f1-5df686bbd97a

Monks, P. S., Archibald, A. T., Colette, A., Cooper, O., Coyle, M., Derwent, R., Fowler, D., Granier, C., Law, K. S., Mills, G. E., Stevenson, D. S., Tarasova, O., Thouret, V., von Schneidemesser, E., Sommariva, R., Wild, O., and Williams, M. L. (2015). Tropospheric ozone and its precursors from the urban to the global scale from air quality to short-lived climate forcer, *Atmos. Chem. Phys*, https://doi.org/10.5194/acp-15-8889-2015.

Morgan, S. (2020), Coronavirus: EU to suspend ‘ghost flights’ rule for 4 months, viewed 1 June 2020, https://www.euractiv.com/section/aviation/news/coronavirus-eu-to-suspend-ghost-flights-rule-for-4-months/

Mulcahy, J. P., Johnson, C., Jones, C. G., Povey, A. C., Scott, C. E., Sellar, A., Turnock, S. T., Woodhouse, M. T., Abraham, N. L., Andrews, M. B., Bellouin, N., Browse, J., Carslaw, K. S., Dalvi, M., Folberth, G. A., Glover, M., Grosvenor, D., Hardacre, C., Hill, R., Johnson, B., Jones, A., Kipling, Z., Mann, G., Mollard, J., O'Connor, F. M., Palmieri, J., Reddington, C., Rumbold, S. T., Richardson, M., Schutgens, N. A. J., Stier, P., Stringer, M., Tang, Y., Walton, J., Woodward, S., and Yool, A. (2020) Description and evaluation of aerosol in UKESM1 and HadGEM3-GC3.1 CMIP6 historical simulations, Geosci. Model Dev. Discuss., https://doi.org/10.5194/gmd-2019-357.

Myhre, G., Samset, B.H., Schulz, M., Balkanski, Y., Bauer, S., Berntsen, T.K., Bian, H., Bellouin, N., Chin, M., Diehl, T. and Easter, R.C. (2013). Radiative forcing of the direct aerosol effect from AeroCom Phase II simulations. *Atmospheric Chemistry and Physics*, https://doi.org/10.5194/acp-13-1853-2013

O'Connor, F. M., Abraham, N. L., Dalvi, M., Folberth, G., Griffiths, P., Hardacre, C., Johnson, B. T., Kahana, R., Keeble, J., Kim, B., Morgenstern, O., Mulcahy, J. P., Richardson, M. G., Robertson, E., Seo, J., Shim, S., Teixeira, J. C., Turnock, S., Williams, J., Wiltshire, A., & Zeng, G. (2020) Assessment of pre-industrial to present-day anthropogenic climate forcing in UKESM1. *Atmos. Chem. Phys. Discuss*. https://doi.org/10.5194/acp-2019-1152, in review.

Sayer, A. M., Hsu, C. N., Bettenhausen, C., Lee, J., Kim, W.V., and Smirnov, A. (2018), Satellite Ocean Aerosol Retrieval (SOAR) Algorithm Extension to S-NPP VIIRS as Part of the “Deep Blue” Aerosol Project, J. Geophys. Res. Atmos., 123, https://doi:10.1002/2017JD027412.

Shi, X. and Brasseur, G.P. (2020).The Response in Air Quality to the Reduction of Chinese Economic Activities during the COVID-19 Outbreak. *Geophysical Research Letters*, https://doi.org/10.1029/2020GL088070

Stevenson, D.S., Doherty, R.M., Sanderson, M.G., Collins, W.J., Johnson, C.E. and Derwent, R.G. (2004). Radiative forcing from aircraft NOx emissions: Mechanisms and seasonal dependence. *Journal of Geophysical Research: Atmospheres*, https://doi.org/10.1029/2004JD004759.

Stevenson, D. S., Young, P. J., Naik, V., Lamarque, J.-F., Shindell, D. T., Voulgarakis, A., Skeie, R. B., Dalsoren, S. B., Myhre, G., Berntsen, T. K., Folberth, G. A., Rumbold, S. T., Collins, W. J., MacKenzie, I. A., Doherty, R. M., Zeng, G., Van Noije, T. P. C., Strunk, A., Bergmann, D., Cameron-Smith, P., Plummer, D. A., Strode, S. A., Horowitz, L., Lee, Y. H., Szopa, 750 S., Sudo, K., Nagashima, T., Josse, B., Cionni, I., Righi, M., Eyring, V., Conley, A., Bowman, K. W., Wild, O. & Archibald, A. (2013) Tropospheric ozone changes, radiative forcing and attribution to emissions in the Atmospheric Chemistry and Climate Model Intercomparison Project (ACCMIP). *Atmos. Chem. Phys.* https://doi:10.5194/acp-13-3063-2013.

Telford, P. J., Braesicke, P., Morgenstern, O., & Pyle, J. A. (2008) Technical Note: Description and assessment of a nudged version of the new dynamics Unified Model. *Atmos. Chem. Phys*. https://doi.org/10.5194/acp-8-1701-2008,

Thornhill, G., Collins, W., Olivié, D., Archibald, A., Bauer, S., Checa-Garcia, R., Fiedler, S., Folberth, G., Gjermundsen, A., Horowitz, L., Lamarque, J.-F., Michou, M., Mulcahy, J., Nabat, P., Naik, V., O'Connor, F. M., Paulot, F., Schulz, M., Scott, C. E., Seferian, R., Smith, C., Takemura, T., Tilmes, S., and Weber, J. (2020) Climate-driven chemistry and aerosol feedbacks in CMIP6 Earth system models. *Atmos. Chem. Phys. Discuss.* https://doi.org/10.5194/acp-2019-1207, in review.

Twomey, S. (1977). The influence of pollution on the shortwave albedo of clouds. *Journal of the atmospheric sciences*. https://doi.org/10.1175/1520-0469(1977)034<1149:TIOPOT>2.0.CO;2

Walters, D., Baran, A. J., Boutle, I., Brooks, M., Earnshaw, P., Edwards, J., Furtado, K., Hill, P., Lock, A., Manners, J., Morcrette, C., Mulcahy, J., Sanchez, C., Smith, C., Stratton, R., Tennant, W., Tomassini, L., Van Weverberg, K., Vosper, S., Willett, M., Browse, J., Bushell, A., Carslaw, K., Dalvi, M., Essery, R., Gedney, N., Hardiman, S., Johnson, B., Johnson, C., Jones, A., Jones, C., Mann, G., Milton, S., Rumbold, H., Sellar, A., Ujiie, M., Whitall, M., Williams, K., and Zerroukat, M. (2019). The Met Office Unified Model Global Atmosphere 7.0/7.1 and JULES Global Land 7.0 configurations, *Geosci. Model Dev*. https://doi.org/10.5194/gmd-12-1909-2019.

World Health Organisation (2020) Coronavirus disease 2019 (COVID-19) Situation Report – 139, viewed 8 June 2020 https://www.who.int/docs/default-source/coronaviruse/situation-reports/20200607-covid-19-sitrep-139.pdf?sfvrsn=79dc6d08_2

Young, P.J., Naik, V., Fiore, A.M., Gaudel, A., Guo, J., Lin, M.Y., Neu, J., Parrish, D., Reider, H.E., Schnell, J.L. and Tilmes, S. (2018). Tropospheric Ozone Assessment Report: Assessment of global-scale model performance for global and regional ozone distributions, variability, and trends. *Elementa: Science of the Anthropocene*, http://doi.org/10.1525/elementa.265

UK Department of Transport (2020). Transport use during the coronavirus (COVID-19) pandemic, https://www.eea.europa.eu/highlights/air-pollution-goes-down-as, viewed 5th April 2020.

Zhang, K., Wan, H., Liu, X., Ghan, S. J., Kooperman, G. J., Ma, P.-L., Rasch, P. J., Neubauer, D., and Lohmann, U. (2014). Technical Note: On the use of nudging for aerosol–climate model intercomparison studies. *Atmos. Chem. Phys*. https://doi.org/10.5194/acp-14-8631-2014.

Zhang, R., Zhang, Y., Lin, H., Feng, X., Fu, T.M. & Wang, Y.. (2020). NOx Emission Reduction and Recovery during COVID-19 in East China. *Atmosphere*. https://doi:10.3390/atmos11040433.

Geophysical Research Letters

Supporting Information for

Minimal climate impacts from short-lived climate forcers following emission reductions related to the COVID-19 pandemic

James Weber[1], Youngsub M. Shin[1], John Staunton Sykes[1], Scott Archer-Nicholls[1], Nathan Luke Abraham[1,2] and Alex T. Archibald[1,2]

[1]Centre for Atmospheric Science, Department of Chemistry, University of Cambridge, Cambridge, CB2 1EW, UK
[2]National Centre for Atmospheric Science, Department of Chemistry, University of Cambridge, Cambridge, CB2 1EW, UK

Contents of this file

Introduction

The following is supporting information for the main text. It consists of additional plots including parameters calculated from processing UKCA output data, additional emission reduction information, further detail as to the calculation of methane concentration perturbation and additional information about the species emitted in the UKCA model.

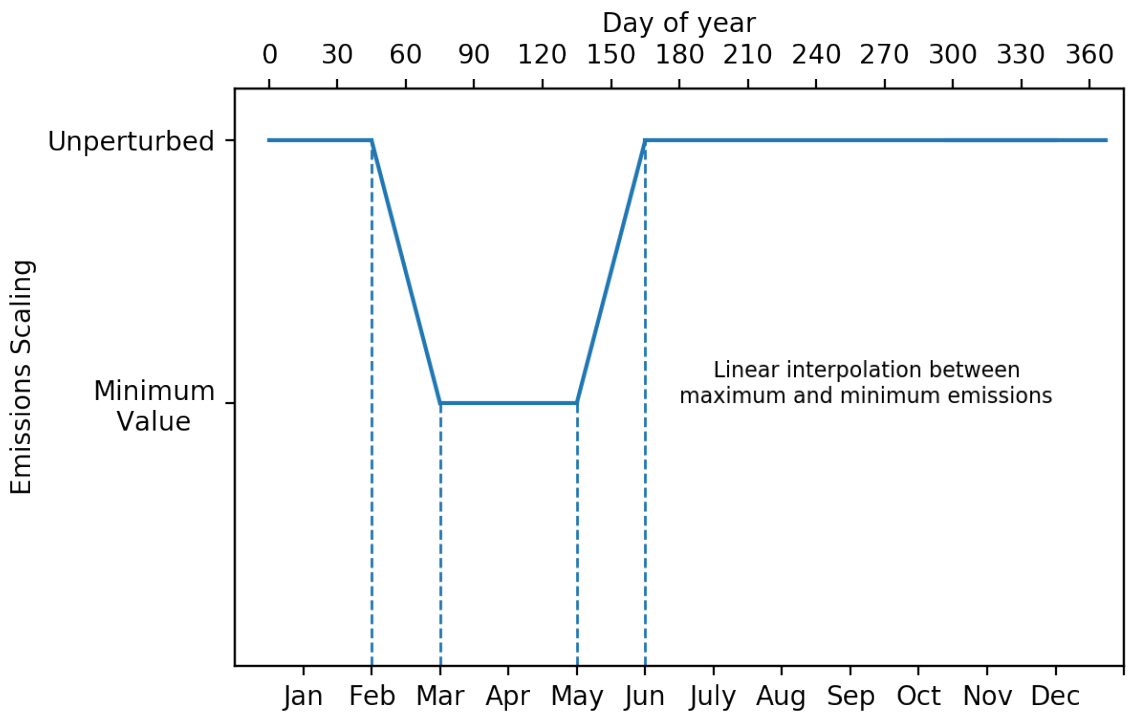

Figure S1. Emissions Time Series. Month ticks aligned to the middle of each month. Emitted values are updated every 5 days.

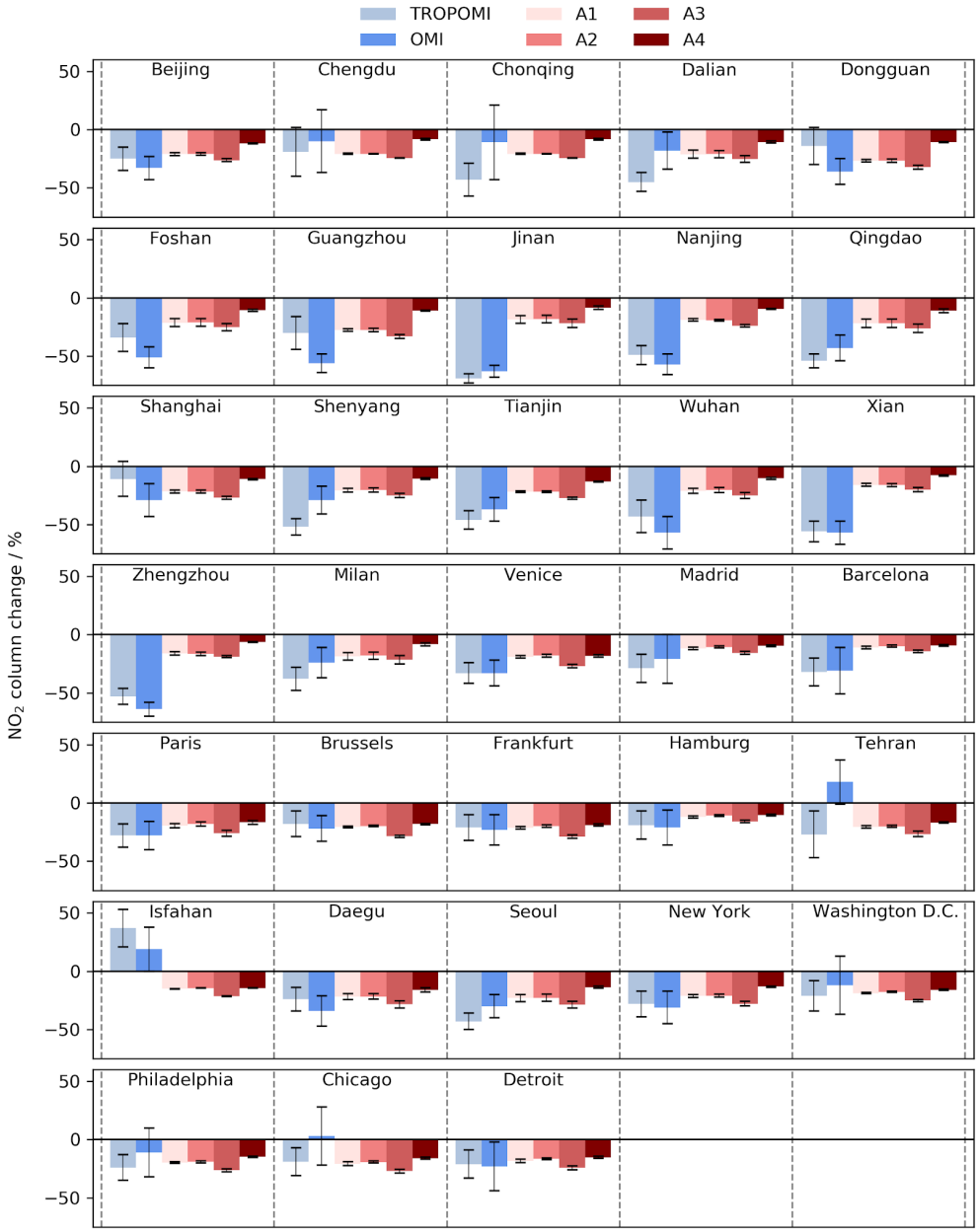

Figure S2. Observed and modelled tropospheric NO_2 column percentage change. Observations are from TROPOMI and OMI for the lockdown period (Feb to Mar) relative to 2019 (Bauwens et al., 2020) and model results from the 4 model scenarios relative to the control averaged over the period of emissions reduction (mid-Mar to mid-May)

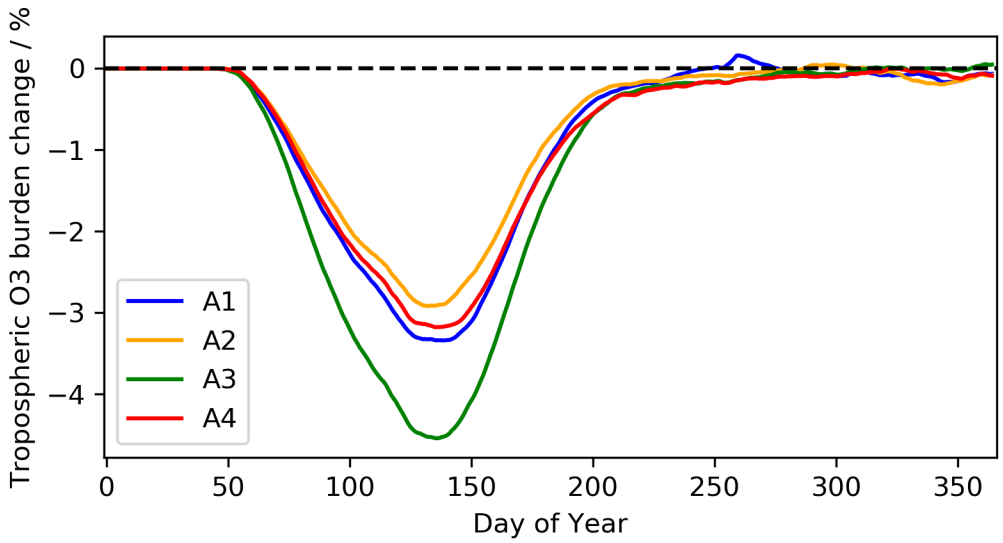

Figure S3. Modelled ensemble mean tropospheric ozone burden change compared to control. Tropopause diagnosed in-model using the WMO thermal lapse-rate tropopause definition (lapse-rate < 2°C km^{-1}).

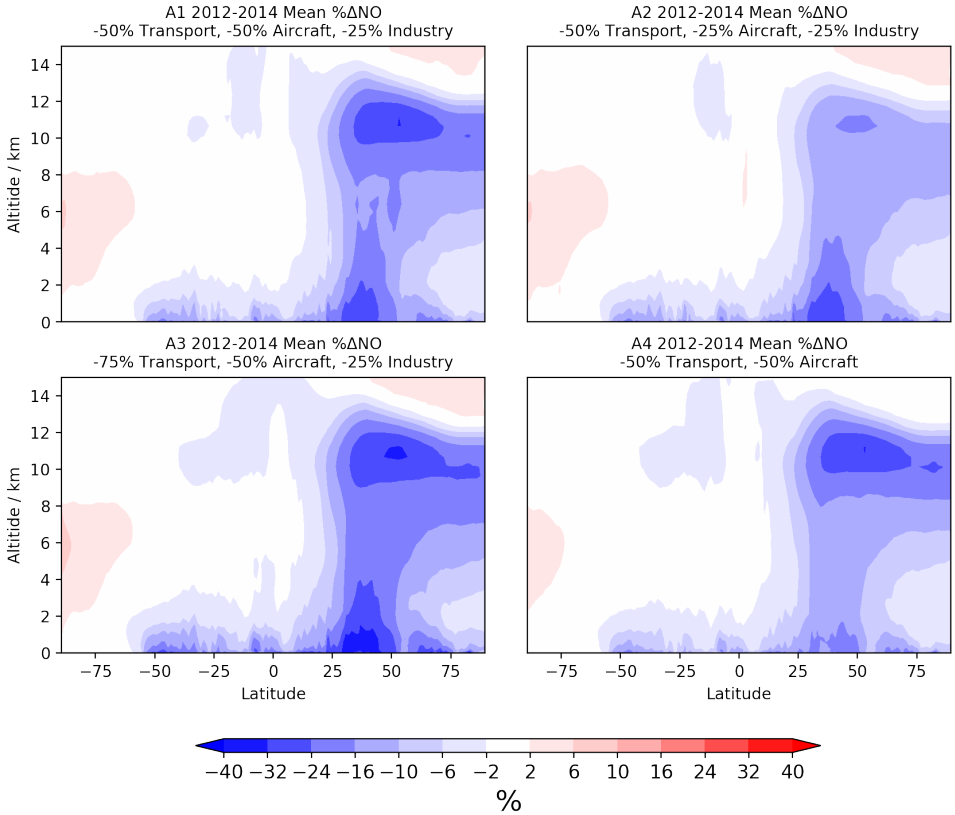

Figure S4. Zonal mean of percentage change in NO mixing ratio (mid March - mid May) averaged over 3 years 2012-2014.

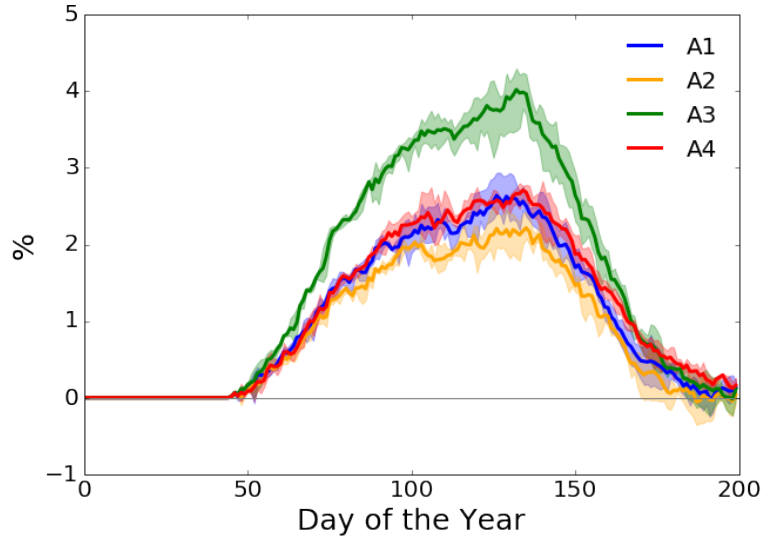

Figure S5. Percentage difference in global mean methane lifetime averaged over 3 years 2012-2014 (shading shows the ensemble range).

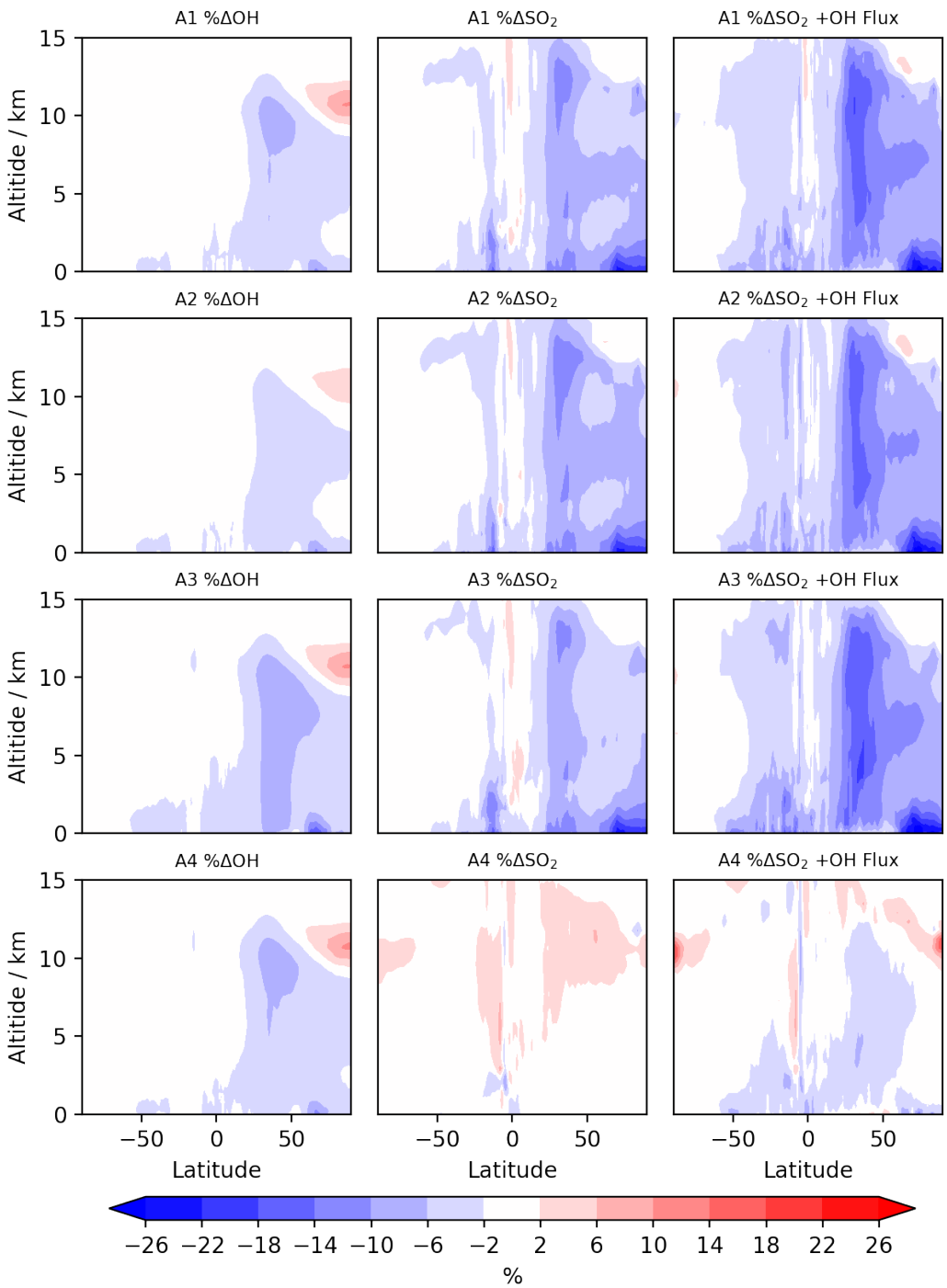

Figure S5. Zonal mean of percentage change in OH and SO_2 mixing ratios and SO_2 + OH flux (mid March - mid May) averaged over 3 years 2012-2014.

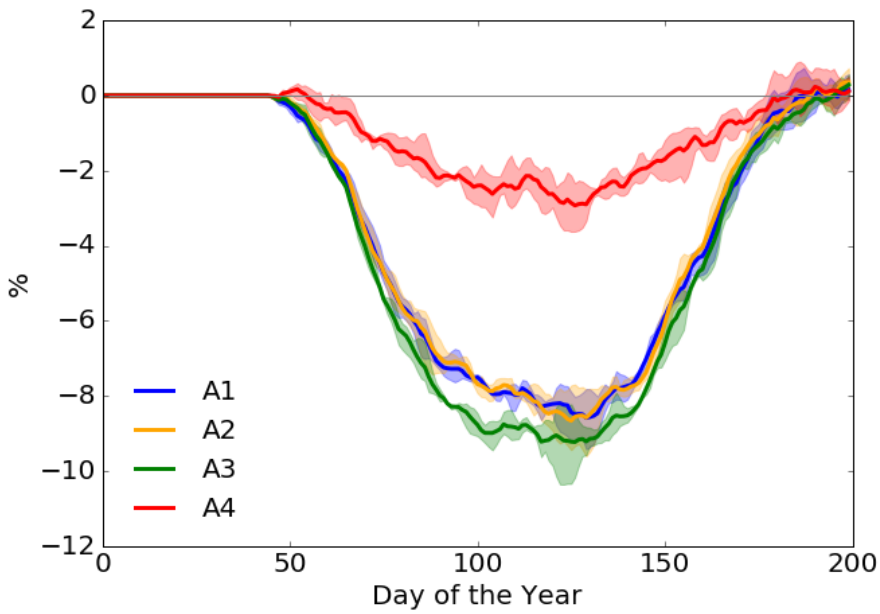

Figure S6. Percentage change time series in total sulfate burden averaged over 3 years 2012-2014. Shading shows ensemble range.

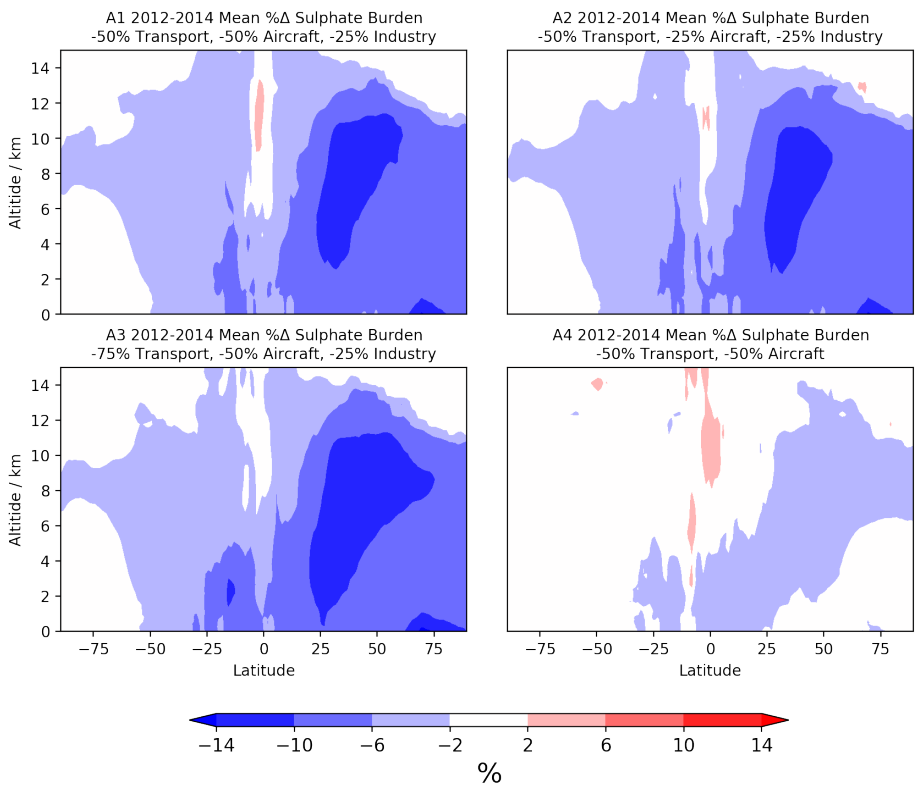

Figure S7. Zonal mean of percentage change in sulphate aerosol burden (mid March - mid May) averaged over 3 years 2012-2014.

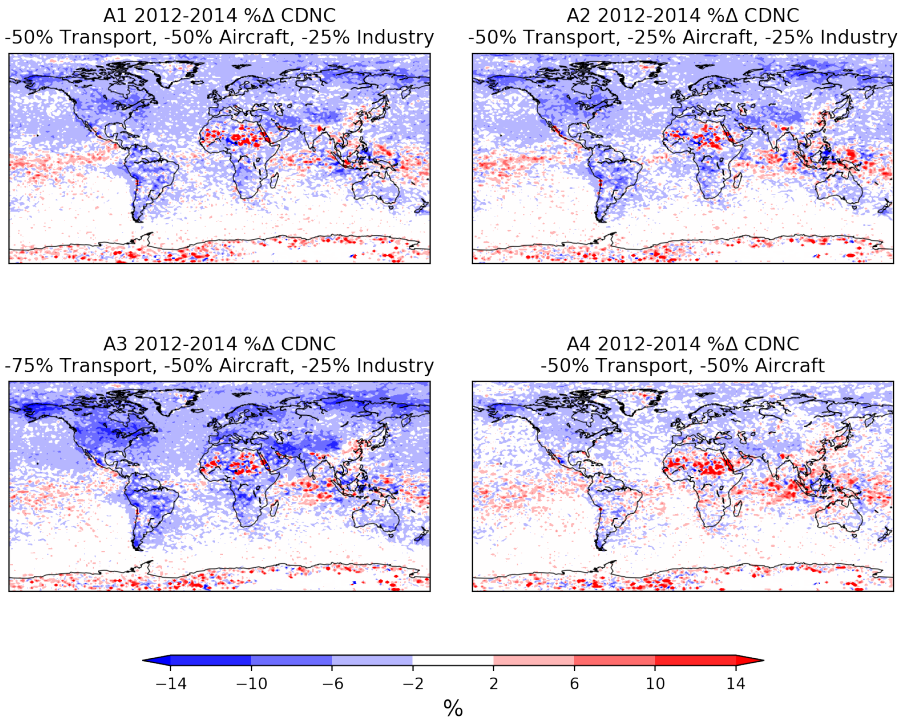

Figure S8. Percentage change in CDNC for (mid March - mid May) averaged over 3 years 2012-2014.

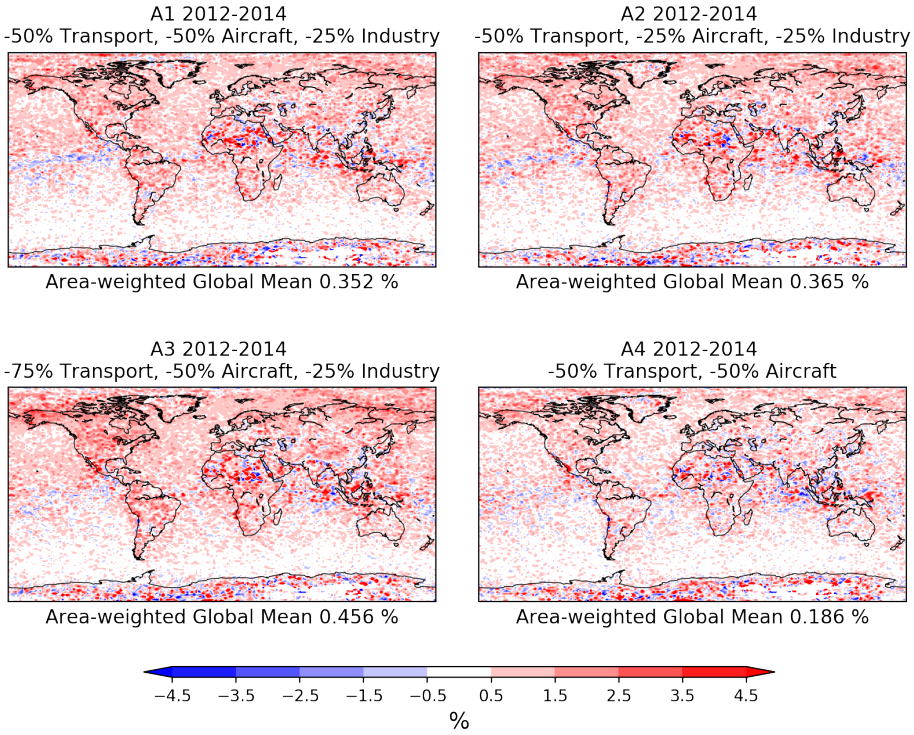

Figure S9. Percentage change in cloud droplet effective radius (mid March - mid May) averaged over 3 years 2012-2014.

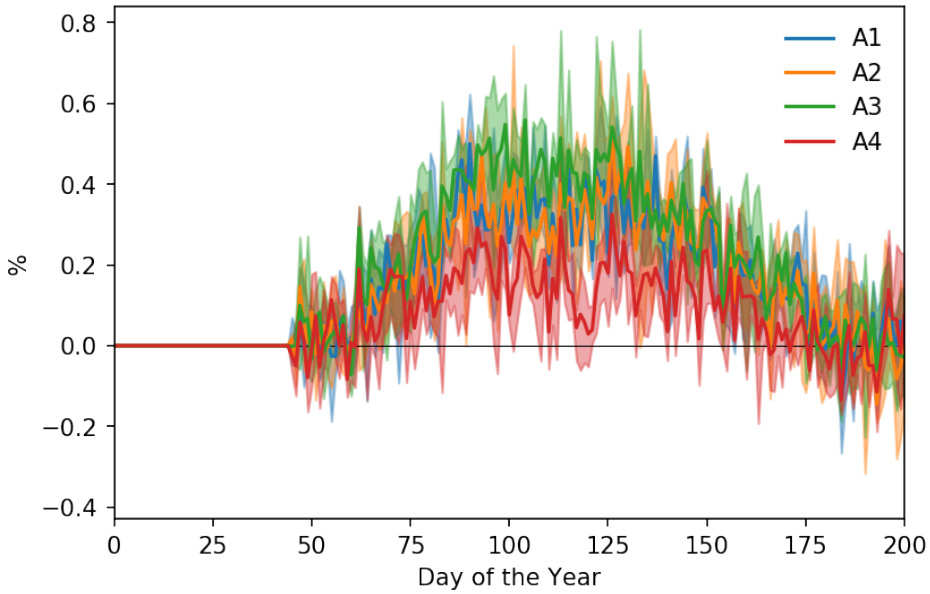

Figure S10. Area-weighted mean percentage change in cloud droplet effective radius (shaded region shows ensemble range). The rapid response to emissions decline and subsequent recovery is evident.

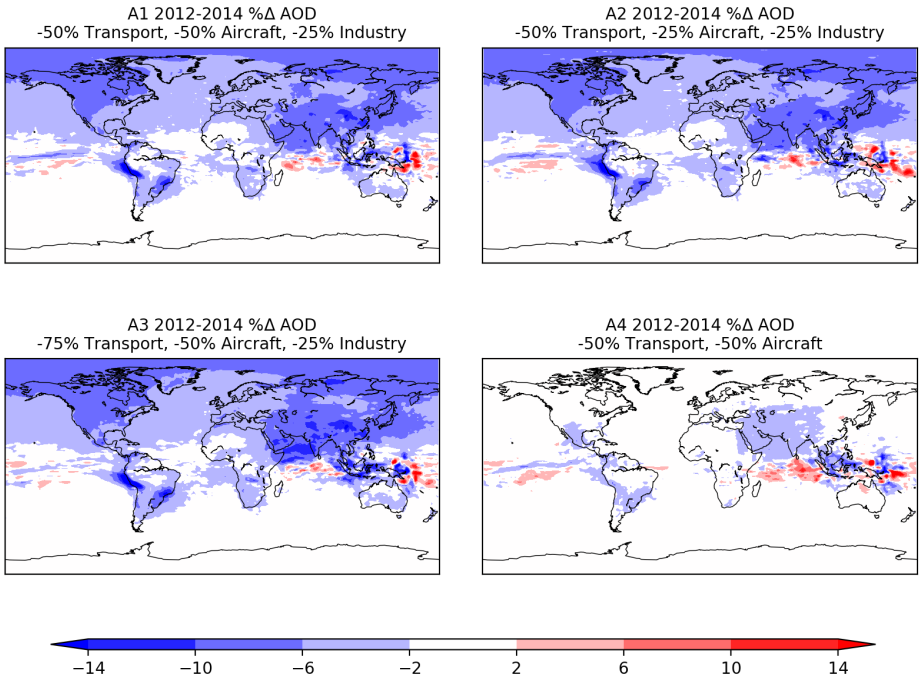

Figure S11. Percentage change in simulated AOD at 550 nm (mid March - mid May) averaged over the three years investigated.

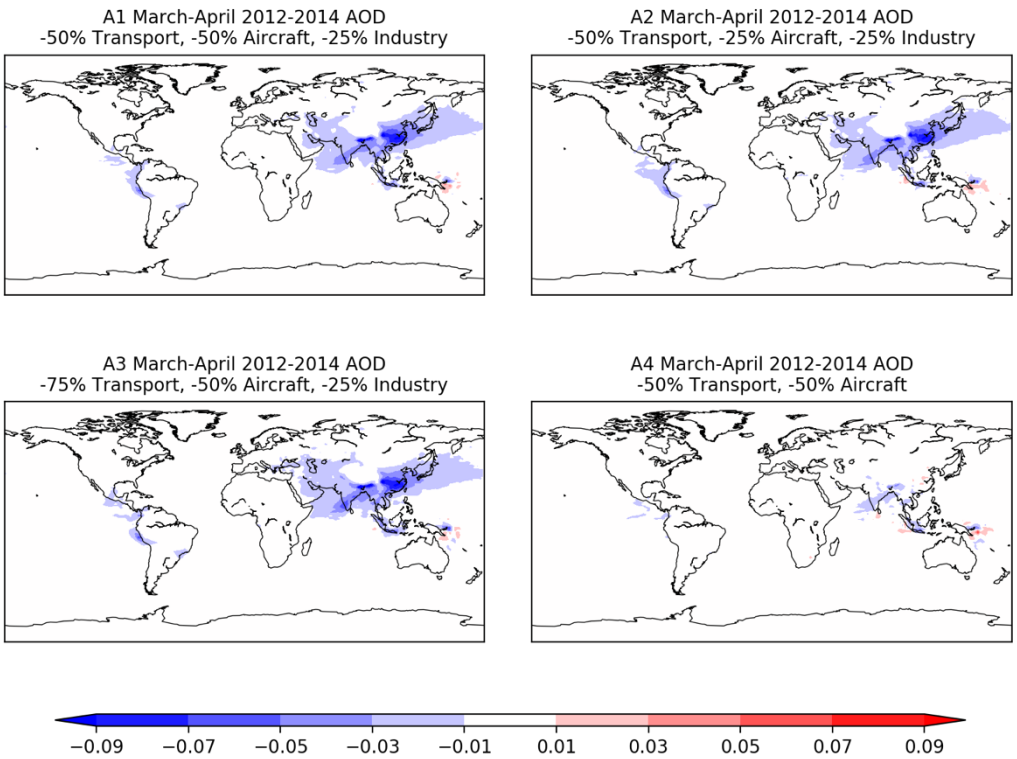

Figure S12. Changes in simulated AOD at 550 nm March-April between perturbed runs and control averaged over 3 years 2012-2014.

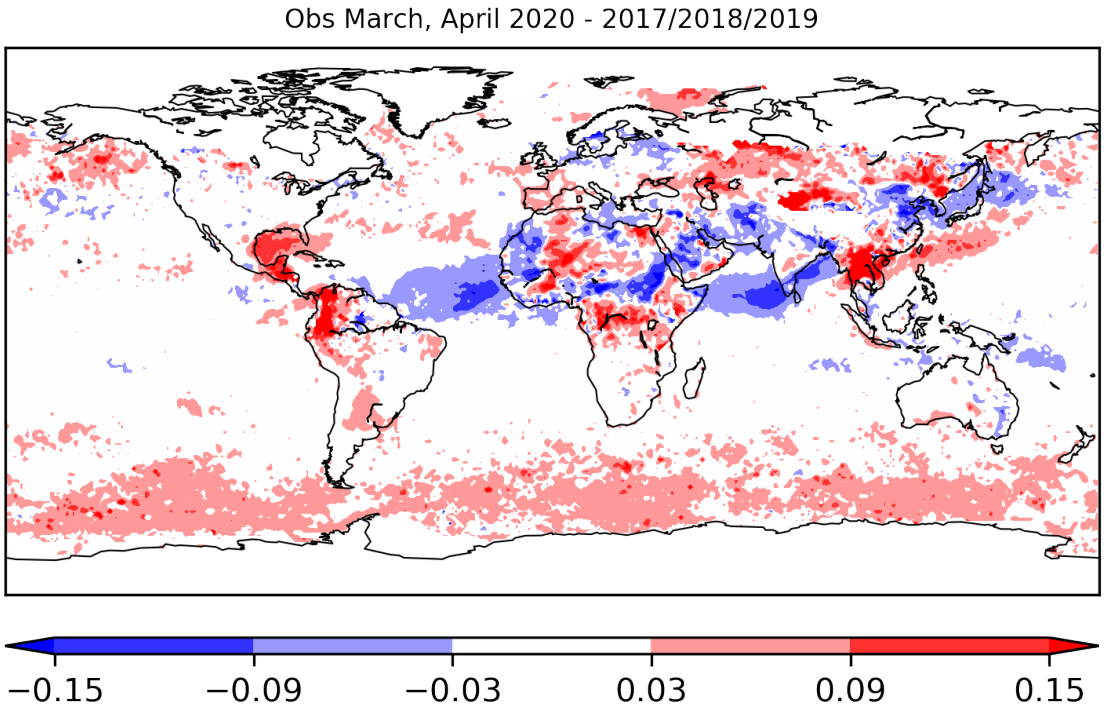

Figure S13. Changes in observed AOD 550 nm from VIIRS (Sayer et al., 2018) between March-April 2020 and mean of March-April 2017-2019.

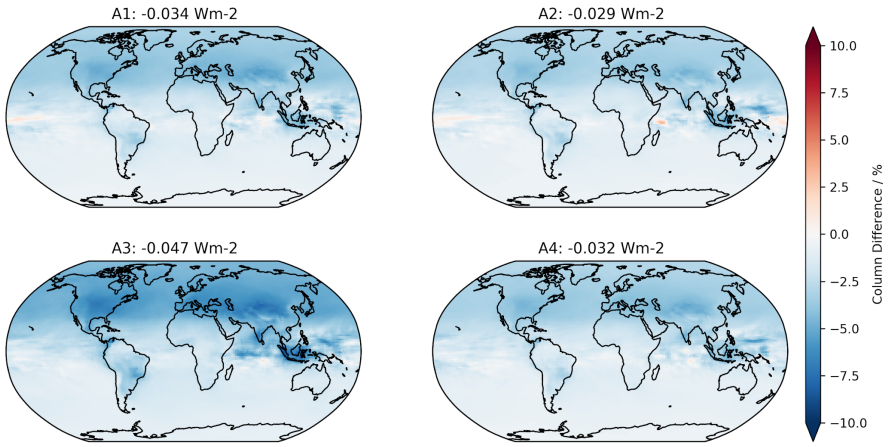

Figure S14. Percentage change in tropospheric O_3 column (mid March - mid May) averaged over 3 years 2012-2014 and instantaneous radiative forcing relative to control calculated using method from Stevenson et al (2013).

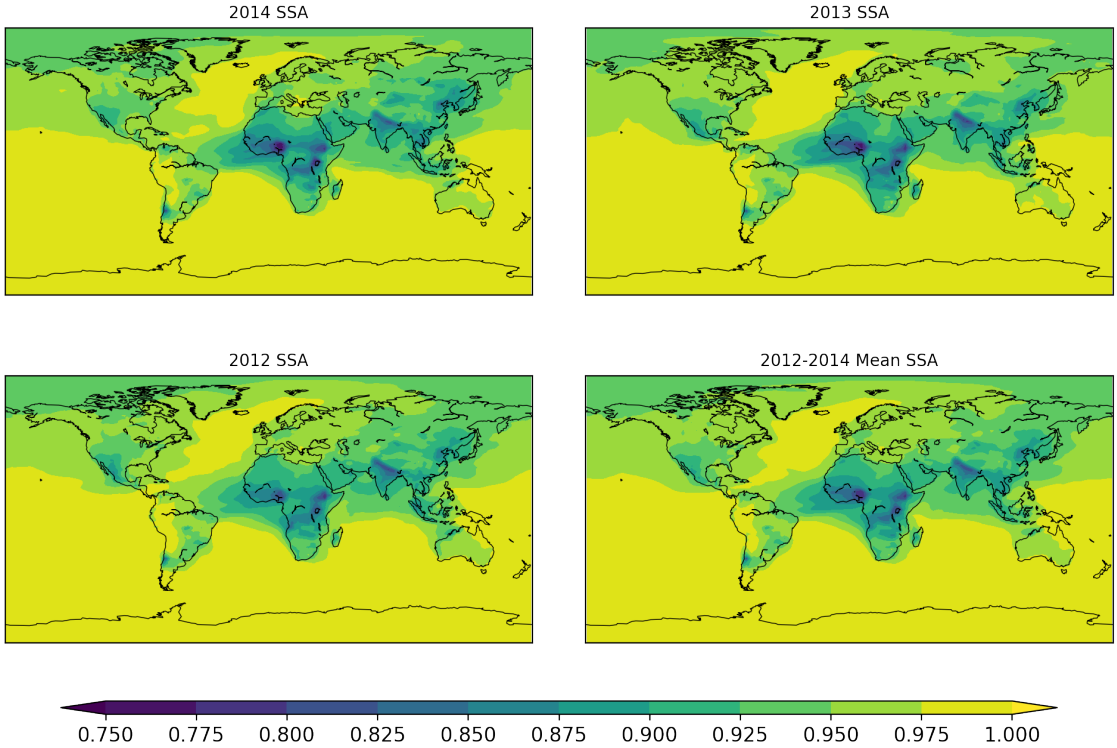

Figure S15. Control single-scattering albedo for individual years and average over 3 years (March-May).

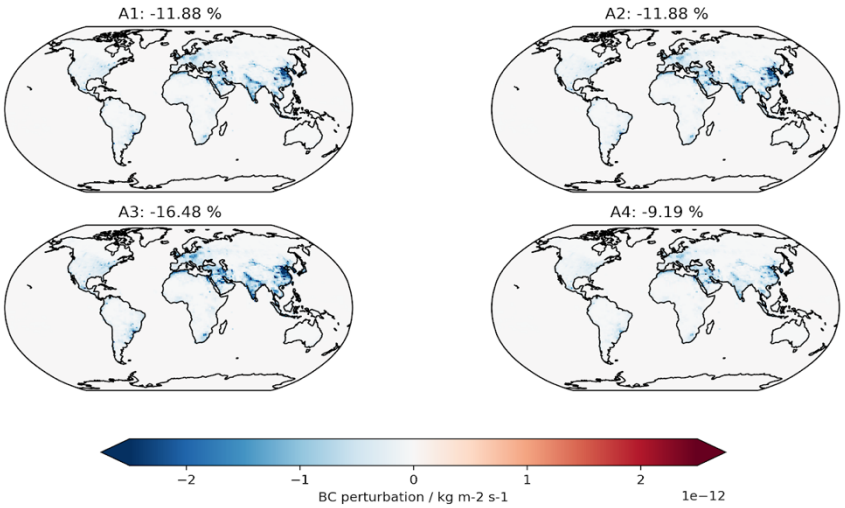

Figure S16. Changes to emissions of black carbon (BC) for March - May averaged over 3 years 2012-2014.

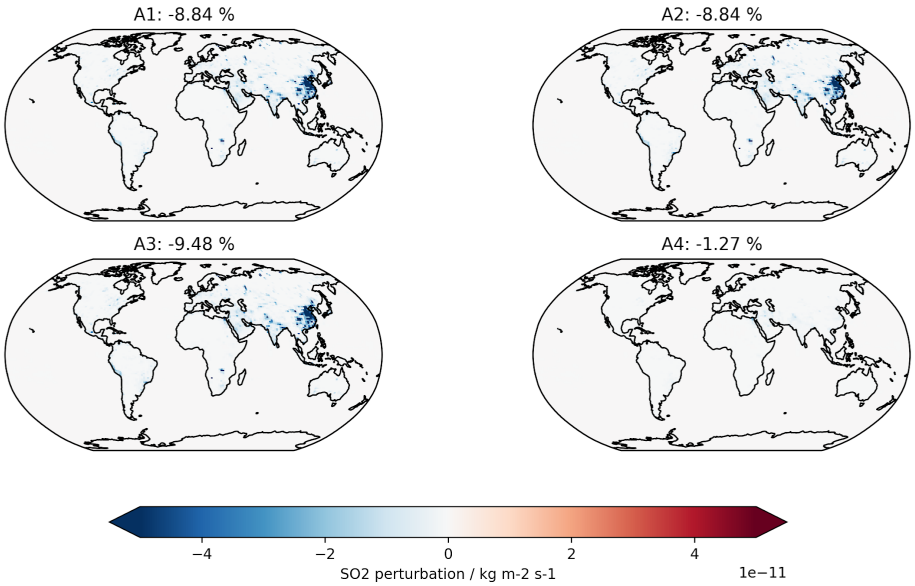

Figure S17. Changes to emissions of SO_2 for March - May averaged over 3 years 2012-2014.

Text S1: Emission Scenario Description

The emissions scenarios were conceptualised in late March/early April 2020 when verified data concerning the impact of lockdowns on anthropogenic sector emissions was not plentiful or widely available. In order to best estimate the reductions, we compiled information from several sources which are detailed below:

Lockdown measures resulted in an 88% decline in car use in the EU and a 60% decrease in industrial carbon emissions by 25th March (Mallet, 2020), the EEA reported that NO2 concentrations in several cities in southern Europe were around 50% lower than 2019 (European Environment Agency, 2020). In the UK, there was a 60% reduction in all motor vehicle use in the UK (UK Department of Transport, 2020).

International flights from the UK, USA, China, Germany and Japan have decreased 75% from January to the end of March this year (Kommenda, 2020), and european internal flights are estimated to have decreased by 86%. Data from Flightradar (FlightRadar, 2020) was also used to estimate a change in the total global flight by around 50%. Some uncertainty was present early on due to the 'ghost flights' berth requirements law, but the law was later suspended (Morgan, 2020).

The industrial sector was also hit by the COVID-19 lockdowns, but was a lot harder to quantify. It was suggested that EU industrial emissions decreased up to 60% [FT 2020],

Whilst it is likely that many other sectors were affected by the lockdowns, the data at the time provided insufficient evidence to come up with perturbations, so we did not attempt to estimate any of these changes. In this manner, our scenarios most likely represent a lower bound on the actual effect.

Text S2: Methane Concentration Evolution

To estimate the transient change in methane as a result of its lifetime perturbation, a simple kinetic model is considered with an instantaneous 4% increase in methane lifetime. This produces an upper bound estimate for methane concentration as the lifetime change in scenarios A1-A4 are not instantaneous and only one scenario, A3, reaches 4% (Fig. S5). Nevertheless, the results are informative.

In this model, the initial steady state concentration of methane, , is defined in terms of methane flux, , and its lifetime, :

$$[CH_4]_0 = F\tau_0$$

Upon an instantaneous perturbation of methane lifetime to perturbed value, , with an unchanged flux, the methane concentration ceases to be that given by the steady state expression and can be described by the following differential equation:

$$\frac{d[CH_4]}{dt} = F - \frac{1}{\tau}[CH_4$$

Solving this via separation of variables yields:

$$-\tau\ ln\ |F - \frac{1}{\tau}[CH_4]| = t + c$$

Where c is the constant of integration.

Noting that at $t = 0$, $[CH_4] = [CH_4]_0$, the constant of integration, c, can be written as

$$c = -\tau\ ln\ |F - \frac{1}{\tau}[CH_4]_0|$$

This yields:

$$-\tau\ ln\ |F - \frac{1}{\tau}[CH_4]| = t - \tau\ ln\ |F - \frac{1}{\tau}[CH_4]_0|$$

Dispensing with the moduli and multiplying by $-\tau$yields:

$$ln\ (F - \frac{1}{\tau}[CH_4]) = -\frac{t}{\tau} + ln\ (F - \frac{1}{\tau}[CH_4]_0)$$

$$F - \frac{1}{\tau}[CH_4] = e^{-\frac{t}{\tau}}(F - \frac{1}{\tau}[CH_4]_0)$$

$$\frac{1}{\tau}[CH_4]=F - e^{-\frac{t}{\tau}}(F - \frac{1}{\tau}[CH_4]_0)$$

$$\frac{1}{\tau}[CH_4]=F(1 - e^{-\frac{t}{\tau}}{}_0) - \frac{1}{\tau}[CH_4]_0 e^{-\frac{t}{\tau}}{}_0$$

$$[CH_4]=F\tau(1 - e^{-\frac{t}{\tau}}{}_0) - [CH_4]_0 e^{-\frac{t}{\tau}}{}_0$$

Noting that $[CH_4]_0 = F\tau_0$

$$[CH_4]=F\tau(1 - e^{-\frac{t}{\tau}}{}_0) - F\tau_0 e^{-\frac{t}{\tau}}{}_0$$

The ratio, r, of perturbed $[CH_4]$to original $[CH_4]_0$ can be expressed as:

$$r = \frac{[CH_4]}{[CH_4]_0}=\frac{F\tau(1-e^{-\frac{t}{\tau}}{}_0)-F\tau_0 e^{-\frac{t}{\tau}}{}_0}{F\tau_0} = \frac{\tau(1-e^{-\frac{t}{\tau}})}{\tau_0} - e^{-\frac{t}{\tau}}$$

This ratio satisfies the requirements:

$$\text{At } t = 0, r = 1$$

$$\text{As } t \to 0, r \to \frac{\tau}{\tau_0}$$

The ratio depends weakly on the initial methane lifetime, but it is clear that several decades are needed for the model to reach a new steady state concentration (Fig. S18). A 4% instantaneous increase in methane lifetime after 3 months, the length of the simulated perturbation, will result in a 0.1% increase in methane concentrations.

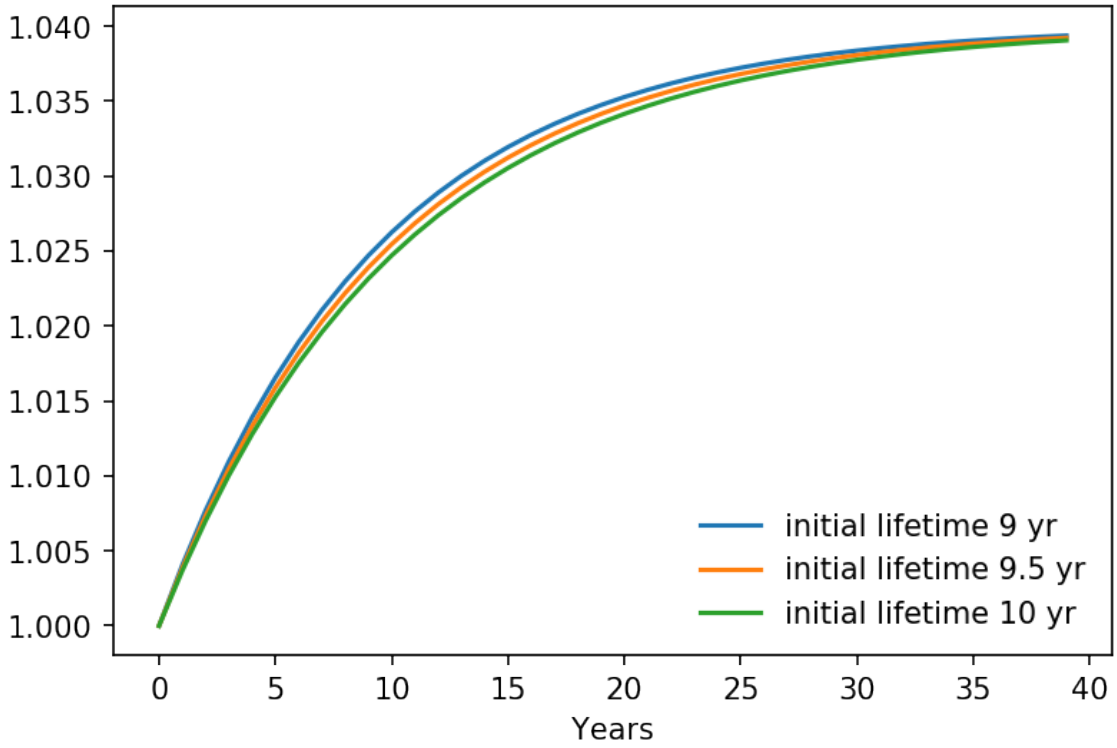

Figure S18. Ratio of perturbed methane concentration to initial methane concentration after an instantaneous increase in methane lifetime of 4% using the simple kinetic framework. Three initial methane lifetimes were considered.

Table S1. Emitted Species

Species
Black carbon
Organic carbon
NO
SO_2
C_2H_6
C_3H_8
HCHO
$(CH_3)_2CO$
CH_3CHO
CH_3OH
Other Organic
NH_3